Quantum Semiclass. Opt. **9** (1997) 867–878. Printed in the UK PII: S1355-5111(97)82066-0

Multi-stability for an extended-cavity diode laser with intracavity atomic absorber

F Di Teodoro†, E Cerboneschi, D Hennequin‡ and E Arimondo
INFM, Dipartimento di Fisica, Università di Pisa, Piazza Torricelli, 2, I-56126 Pisa, Italy

Received 21 February 1997

Abstract. Either single- or multi-mode emission from a diode laser coupled to an external cavity containing a cell filled with caesium vapour has been observed. The oscillation frequency of each operating mode of the laser is locked to a hyperfine transition or crossover resonance of the saturated absorption spectrum of the caesium D_2 line. A model based on the rate equations for external-feedback diode lasers, modified in order to include frequency-dependent losses and dispersion of the laser field through the atomic absorber, has been developed. We show that the atomic absorption resonances determine the lasing frequencies. A multi-stable behaviour is obtained.

1. Introduction

In recent years, diode lasers exposed to optical feedback from an external cavity containing an atomic absorber have been widely investigated, mainly for the purpose of improving the spectral performance of the lasers and achieving an absolute frequency stabilization, for applications, for instance, in optical communications, high-resolution spectroscopy and metrology. The D_2 absorption lines of Cs and Rb atoms lie within the gain curve of conventional diode lasers. The incorporation of a cell of these atomic vapours in an external cavity optically coupled to a diode laser provides dispersive losses. The resulting frequency-dependent changes of the laser gain and refractive index allow one to lock the laser frequency to the atomic resonances and to correct for amplitude and phase fluctuations of the laser field [1]. Frequency locking and quenching of the spectral linewidth have been achieved by employing high-contrast sub-Doppler atomic resonances as dispersive loss mechanisms. Different optical methods have been developed to generate these resonances within a feedback cavity, such as techniques of saturation spectroscopy [2], Faraday rotation [3, 4], resonant phase conjugation [5], velocity-selective optical pumping [6] and Doppler-free collinear polarization spectroscopy [7].

In this paper, we report on spectral measurements performed on an extended-cavity diode laser containing a Cs cell in a saturation spectroscopy configuration similar to that discussed in [2]. In the feedback scheme considered, the light field emitted from the output facet of the diode laser, tuned to the D_2 line, passes through the atomic vapour cell as a pump field and, after being attenuated by the vapour, is retroreflected and used as a counterpropagating probe field, which is fed back into the laser cavity. At the centre of

† Present address: Physics Department, Bryn Mawr College, Bryn Mawr, PA 19010-2899, USA.
‡ Permanent address: Laboratoire de Spectroscopie Hertzienne, Unité associée au CNRS, Université des Sciences et Technologies de Lille, 59655 Villeneuve d'Ascq Cedex, France.

1355-5111/97/050867+12$19.50

any hyperfine transition of the D_2 absorption line, the pump beam bleaches a hole in the absorption spectrum of the weaker probe beam. Therefore, the probe transmission, and hence the optical feedback intensity, is resonantly enhanced when the laser frequency matches one of the principal transition or crossover lines. The saturated medium also modifies, due to its dispersive properties, the feedback phase. As an effect of the frequency-dependent changes produced by the intracavity absorber on the feedback parameters, we observe single-mode emission with frequency locking to an atomic resonance, as well as multi-mode operation with each oscillation frequency corresponding to a different sub-Doppler feature of the atomic absorption spectrum.

A diode laser subject to optical feedback from an external reflector is a multi-stable system, with regard to the selection of the external-cavity modes [8, 9]. Depending on the feedback conditions, the coexistence of several longitudinal modes involves either mode-hopping instabilities [10] or chaotic temporal dynamics [11–13]. To understand how the presence of an intracavity atomic absorber modifies the mode structure of the extended-cavity diode laser, we have generalized the Lang–Kobayashi equations [9] in order to include the dependence of the feedback parameters on the laser frequency and analysed the steady-state solutions of these equations. A similar approach has been used in [1, 3], to explain the occurrence of frequency locking to an atomic resonance and linewidth reduction of the laser emission. In these works, a single Doppler-free resonance has been considered. In this paper we include, in the laser rate equations, the dependence of the feedback intensity and phase on the whole spectrum of the D_2 line and demonstrate that, under certain operating conditions, more than one sub-Doppler resonance can satisfy the lasing conditions.

This paper is organized as follows. In section 2 we describe the experimental apparatus and present the observed optical spectra. In section 3 we introduce the rate equations with frequency-dependent feedback parameters and discuss their steady-state solutions. We focus on the diode laser physics, but also include a short description of the calculation of the saturated absorption and dispersion coefficients of the Cs atoms. Conclusions and final remarks are presented in section 4.

2. Experiment

2.1. Apparatus

The experimental set-up is shown schematically in figure 1. The observations were performed using a Spectra Diode Laser SDL-5400, oscillating at a wavelength around 850 nm. The laser was optically coupled, through an antireflection-coated collimating objective, to an external cavity terminated by a 1200 line/mm Littrow-mounted diffraction grating, placed 46 cm from the laser. A 4 cm long cell containing Cs vapour at the equilibrium density at room temperature was inserted within the external cavity. A fraction of the laser intensity was extracted from the external cavity by means of a beamsplitter with less than 10% reflectivity and used for the detection. To avoid unwanted feedback from optical surfaces in the measuring equipment, the extracted beam propagated through a magneto-optical isolator providing 40 dB of attenuation for counterpropagating light. A scanning confocal Fabry–Perot spectrum analyser, model 240 by Coherent, with a free spectral range $\Delta\nu_{FP} = 1.5$ GHz, detected the optical spectrum of the laser emission. Absolute optical frequency measurements were performed by comparison with the oscillation frequency of a reference diode laser, locked, through a standard technique of hybrid optical and electronic feedback [14], to the $F = 4 \rightarrow F' = 5$ transition of the D_2 Cs line.

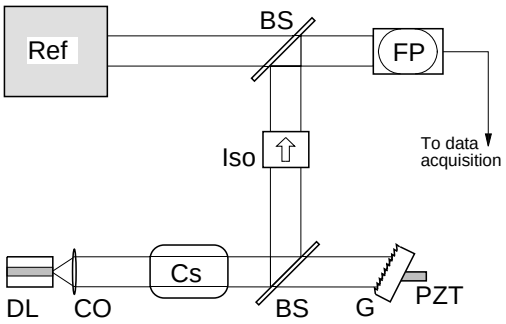

Figure 1. Scheme of the experimental set-up. DL, diode laser; CO, collimating objective; Cs, caesium cell; BS, beamsplitter; G, diffraction grating; PZT, piezoelectric transducer; Iso, magneto-optical isolator; Ref, reference diode laser; FP, scanning confocal Fabry–Perot spectrum analyser.

The diffraction grating terminating the external cavity was mounted on a piezoelectric transducer, fixed to a mirror mounting. Continuous tuning of the laser wavelength within a range of tens of nanometres was achieved by combining the rotation of the grating and the variation of the cavity length through the piezoelectric transducer. For laser frequencies far from the Doppler-broadened absorption line of the atoms, the feedback power ratio was estimated, including losses at the optical surfaces within the external cavity, as about 30%.

2.2. Self-locking and multi-mode emission

By tuning the laser frequency, through the rotation and fine translation of the grating, to the hyperfine transition $F = 4 \rightarrow F' = 5$, we observed monomode self-locked operation. In figure 2, the detuning between the oscillation frequency of the laser and the line centre of the atomic transition is plotted as a function of the voltage applied to the piezoelectric transducer, which scans the length of the external cavity. The detuning values were measured from the optical Fabry–Perot spectra. The curve is composed of two identical branches, since two free spectral ranges of the external cavity are scanned by the total voltage variation. Measurements performed far from the atomic absorption lines showed that the laser frequency, when unlocked, changed almost linearly with the applied voltage, with a slope of ~ 80 MHz V^{-1}. Figure 2 shows, instead, that at the atomic line centre the frequency was insensitive to voltage changes. Thus, the laser mode jumped onto the resonance and remained locked there, while it would otherwise be scanning. The flat part of the curve covers a voltage interval of about 2 V, which would correspond, out of resonance, to a frequency change of $\sim$160 MHz. This value represents the locking range around the atomic transition. Figure 2 shows a slight variation of the laser frequency within the locking range.

Out of the locking range, we observed multi-mode emission, as demonstrated by the multi-peaked optical spectra shown in figure 3. These spectra were obtained by scanning the external-cavity length, so as to move the laser frequency out of the $F = 4 \rightarrow F' = 5$ line in the low-frequency direction. Figure 3(a) shows the simultaneous excitation of several frequencies separated by 320 MHz, corresponding to the free spectral range $\Delta\nu_{ex}$ of the external cavity. In this situation, the mode selection is dominated by the optical properties of the empty cavity and appears not to be modified by the presence of the atomic absorber.

The grating providing the external feedback has a very low resolving power, compared to the FSR of the external cavity, so that it cannot select a single mode. The simultaneous

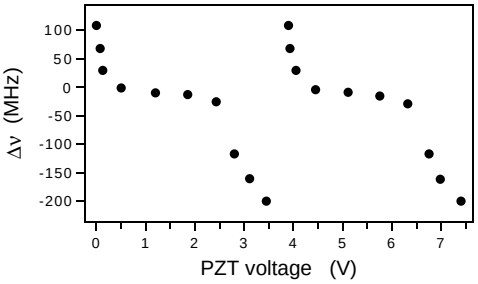

Figure 2. Tuning of the laser frequency versus the external-cavity length scanned by application of a voltage to the piezoelectric transducer. $\Delta\nu$ indicates the difference between the laser frequency and the frequency of the D_2 hyperfine $F = 4 \rightarrow F' = 5$ transition in caesium. Two free spectral ranges of the external cavity are scanned by the total voltage variation. The plateaux indicate self-locking of the laser frequency to the resonance of the intracavity atomic absorber.

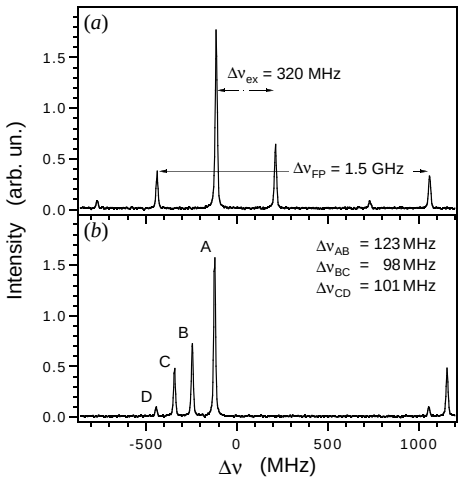

Figure 3. Optical power spectra of the laser emission obtained from a Fabry–Perot scan. Laser multi-mode operation is present with oscillation frequencies resonant in (*a*) with the empty-cavity $\Delta\nu_{ex}$ frequencies and in (*b*) with Lamb dips and crossover resonances of the saturated absorption spectrum of the intracavity atomic vapour. $\Delta\nu$ denotes the laser detuning from the D_2 $F = 4 \rightarrow F' = 5$ transition. The free-spectral range of the external cavity, $\Delta\nu_{ex}$, and of the Fabry–Perot, $\Delta\nu_{FP}$, are denoted.

excitation of several external-cavity modes in a diode laser exposed to optical feedback from a diffraction grating was reported, for instance, in [15].

In the situation illustrated in figure 3(*b*), where the laser frequency was within the Doppler linewidth of the D_2 transitions, the absorber determines entirely the selection of the laser frequencies. Each laser frequency corresponded, within the 10 MHz resolution of the Fabry–Perot spectrum analyser, to a different sub-Doppler resonance of the D_2 absorption spectrum [16]. Inside the external cavity which provided the feedback to the diode laser, two counterpropagating laser beams, oscillating at the same frequency, excited the Cs vapour in a saturation spectroscopy configuration [16, 17]. The D_2 hyperfine transitions involved in figure 3(*b*) are from the ground hyperfine state $F = 4$ to the excited hyperfine states $F' = 3, 4$ and 5. An energy level scheme of the Cs D_2 line is shown in figure 4, where the principal Lamb dips and the crossover resonances are shown. The numerical values for the spectroscopic parameters relative to the considered Cs transitions can be found, for instance, in [16]. In figure 3(*b*), the detuning of peak A, with respect to the reference $F = 4 \rightarrow F' = 5$ frequency, matched the position of the crossover resonance involving the transitions from $F = 4$ to $F' = 4, 5$. Peak B corresponded to the $F = 4 \rightarrow F' = 4$ Lamb dip, C to the $F = 4 \rightarrow F' = 3, 4$ crossover resonance and D to the $F = 4 \rightarrow F' = 3$ Lamb dip.

Similar spectral observations were also performed with an external-cavity length of 68 cm, corresponding to an FSR of 220 MHz. We have verified that, while the frequency separation of the modes associated with the empty external cavity changed accordingly, the spectrum of the multi-mode emission induced by the absorber was unaffected by the change of the cavity length.

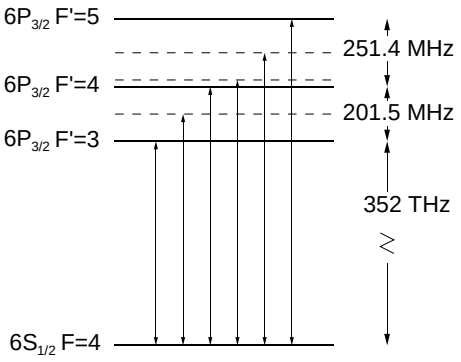

Figure 4. Partial energy diagram of the levels participating in the caesium D_2 absorption spectrum explored in the present work. Vertical lines indicate Lamb dips and crossover resonances. The crossover resonances occur for a laser detuning halfway between the frequencies of neighbouring Lamb dips, as shown by the broken curves.

3. Theory

3.1. Saturated absorption and dispersion coefficients of caesium atoms

We calculated numerically, from the density matrix equations, the absorption and dispersion coefficients associated with both the pump and probe fields. The laser electric field is assumed to propagate in the z-direction and its complex amplitude is written as

$$\mathcal{E}(z,t) = E^{+}(z,t)\mathrm{e}^{-\mathrm{i}(\omega t - kz)} + E^{-}(z,t)\mathrm{e}^{-\mathrm{i}(\omega t + kz)} \tag{1}$$

where E^{+} is the saturating pump field and E^{-} is the probe field. For the atomic density matrix ρ, the following notation is used:

$$\rho_{i'4} = \sigma^{+}_{i'4}(z,t)\mathrm{e}^{-\mathrm{i}(\omega t - kz)} + \sigma^{-}_{i'4}(z,t)\mathrm{e}^{-\mathrm{i}(\omega t + kz)} \tag{2}$$

where $\rho_{i'4}$ are the off-diagonal matrix elements corresponding to the optical transitions $4 \to i'$ ($i' = 3', 4'$ and $5'$).

In the rotating-wave and slowly varying envelope approximations, the density matrix equations are

$$\frac{\partial \sigma^{\pm}_{i'4}}{\partial t} = \left(\mathrm{i}\Delta^{\pm}_{i'4} - \gamma_{i'4}\right)\sigma^{\pm}_{i'4} - \frac{\mathrm{i}E^{\pm}}{\hbar}\left[d_{i'4}(\rho_{i'i'} - \rho_{44}) + \sum_{j' \neq i'} d_{j'4}\rho^{*}_{j'i'}\right] \tag{3a}$$

$$\frac{\partial \rho_{i'j'}}{\partial t} = -(\mathrm{i}\omega_{i'j'} + \gamma_{i'j'})\rho_{i'j'} - \frac{\mathrm{i}}{\hbar}\left[d_{j'4}\left(E^{+*}\sigma^{+}_{i'4} + E^{-*}\sigma^{-}_{i'4}\right) - d_{i'4}\left(E^{+}\sigma^{+\,*}_{j'4} + E^{-}\sigma^{-\,*}_{j'4}\right)\right] \tag{3b}$$

$$\frac{\partial \rho_{i'i'}}{\partial t} = -(\Gamma_{i'} + \gamma_r)\rho_{i'i'} + \frac{2d_{i'4}}{\hbar}\,\mathrm{Im}\left\{E^{+*}\sigma^{+}_{i'4} + E^{-*}\sigma^{-}_{i'4}\right\} \tag{3c}$$

$$\frac{\partial \rho_{44}}{\partial t} = \gamma_r\left(\rho^{0}_{44} - \rho_{44}\right) + \sum_{i'}\left(r_{i'4}\Gamma_{i'}\rho_{i'i'} - \frac{2d_{i'4}}{\hbar}\,\mathrm{Im}\left\{E^{+*}\sigma^{+}_{i'4} + E^{-*}\sigma^{-}_{i'4}\right\}\right) \tag{3d}$$

with $i' \neq j'$ and $i', j' = 3', 4'$ and $5'$. The detuning coefficients $\Delta^{\pm}_{i'4}$ are defined as

$$\Delta^{\pm}_{i'4} = \left(1 \mp \frac{v}{c}\right)\omega - \omega_{i'4} \tag{4}$$

where v is the z-component of the atom velocity and $\omega_{i'4}$ is the angular-frequency separation of levels i' and 4. An atom moving towards the pump beam with velocity v sees its frequency upshifted by an amount $(\omega v)/c$ (to lowest order in v/c) while the frequency of the probe beam is, for the same atom, downshifted by an amount $-(\omega v)/c$. In equations (3), the angular-frequency separation of upper levels i' and j' is indicated as $\omega_{i'j'}$. The decay

rates of the off-diagonal density matrix elements are defined as $\gamma_{i'4} = \Gamma_{i'}/2 + \gamma_r$ and $\gamma_{i'j'} = (\Gamma_{i'} + \Gamma_{j'})/2 + \gamma_r$, where $\Gamma_{i'}$ is the natural linewidth of level i' and γ_r is the inverse mean transit time of an atom moving at thermal velocity through the laser beam section. The rate γ_r [16] describes the injection of fresh atoms into the interaction region, as well as the loss of interacting atoms. For atoms entering the beam in thermal equilibrium, only the population ρ_{44}^0, assumed to be proportional to the Zeeman degeneracy of the ground state, is different from zero. The coefficient $d_{i'4}$ denotes the dipole matrix element and $r_{i'4}$ the branching ratio relative to the transition $4 \rightarrow i'$. Equations (3) allow for the simultaneous interaction of the two counterpropagating laser fields with all hyperfine transitions $4 \rightarrow 3', 4'$ and $5'$, so that coherent effects related to the excitation of the atomic coherences between excited states, which are not negligible for a detuned atom–field interaction, are taken into account. This four-level model leads to a satisfactory agreement with the saturated absorption spectra commonly observed in the configuration considered.

The density matrix is a function of the atomic velocity v, which appears explicitly in equations (3) through the detuning coefficients $\Delta_{i'4}^{\pm}$. If the number of atoms per unit volume with velocity v is $N(v)\,\mathrm{d}v$, their contribution to the spatio-temporal field evolution is, from the Maxwell equations,

$$\left(\frac{\partial}{\partial z} + \frac{1}{c}\frac{\partial}{\partial t}\right)E^{\pm} = \mathrm{i}\frac{4\pi\omega}{c}\left[\sum_{i'} d_{i'4}\sigma_{i'4}^{\pm}(v)\right]N(v)\,\mathrm{d}v \tag{5}$$

with $i' = 3', 4'$ and $5'$. According to equation (5), the absorption and dispersion coefficients for the field amplitudes $E^{\pm}$ are defined as

$$\alpha^{\pm} = \mathrm{Im}\left\{\frac{1}{E^{\pm}}\left[\frac{4\pi\omega}{c}\int\sum_{i'} d_{i'4}\sigma_{i'4}^{\pm}(v)N(v)\,\mathrm{d}v\right]\right\} \tag{6a}$$

$$\beta^{\pm} = \mathrm{Re}\left\{\frac{1}{E^{\pm}}\left[\frac{4\pi\omega}{c}\int\sum_{i'} d_{i'4}\sigma_{i'4}^{\pm}(v)N(v)\,\mathrm{d}v\right]\right\}. \tag{6b}$$

The steady-state solution for the optical atomic coherences $\sigma_{i'4}^{\pm}$ was computed numerically from equations (3) for different fixed values of the laser oscillation frequency ω and the atomic velocity v, and the coefficients $\alpha^{\pm}$ and $\beta^{\pm}$, as functions of ω, were obtained from equations (6) by integration over the velocity distribution, assumed to be Maxwellian,

$$N(v) = \frac{N_0}{u\sqrt{\pi}}\mathrm{e}^{-(v/u)^2} \tag{7}$$

with N_0 the total atomic density and $u/\sqrt{2}$ the root-mean-square atomic velocity.

The resulting spectra for the absorption and dispersion coefficients of the probe field are shown in figure 5. The calculation was performed for a pump beam intensity of $0.6I_s$, with I_s the saturation intensity of the transition $4 \rightarrow 5'$, and a probe beam intensity of $0.02I_s$. These values conform with the experimental conditions. For the atomic density, the value $N = 5 \times 10^{10}$ cm^{-3}, of equilibrium at room temperature, was assumed. The narrow features which appear in the spectra correspond to the Lamb dips and the crossover resonances. Within these resonances, the absorption of the probe is considerably reduced and the refractive index changes rapidly. The corresponding spectra for the pump field, not shown here, do not present any sub-Doppler structure. The calculated coefficients were used to characterize the global dependence of the external-cavity round-trip losses and the phase change on the laser frequency, within the D_2 line.

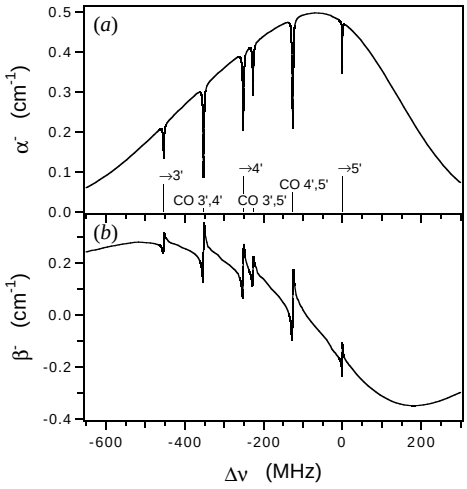

Figure 5. Calculated coefficients of (*a*) absorption and (*b*) dispersion of the D_2 $F = 4 \rightarrow F' = 3, 4$ and 5 transitions of Cs atoms for the probe field in a saturation spectroscopy configuration. Lamb dips and crossover resonances (CO) are labelled by the corresponding upper hyperfine states.

3.2. Rate equations for a diode laser with frequency-dependent optical feedback

The behaviour of a diode laser with external optical feedback is described by the Lang–Kobayashi rate equations [9], for the slowly varying complex field envelope $E(t)$ and the number of charge carriers in the active layer $N(t)$,

$$\frac{\partial E(t)}{\partial t} = \frac{1}{2}(1 + \mathrm{i}\alpha)\Gamma G_N[N(t) - N_{\mathrm{th}}]E(t) + \frac{\kappa}{\tau_{\mathrm{in}}}\mathrm{e}^{\mathrm{i}\omega_0\tau}E(t-\tau) \tag{8a}$$

$$\frac{\partial N(t)}{\partial t} = J - \frac{N(t)}{\tau_{\mathrm{e}}} - \left\{\frac{\Gamma_0}{\Gamma} + G_N[N(t) - N_{\mathrm{th}}]\right\}|E(t)|^2. \tag{8b}$$

Here, the complex electric field amplitude is written as $\mathcal{E}(t) = E(t)\exp(-\mathrm{i}\omega_0 t)$, with ω_0 the angular oscillation frequency of the solitary laser and normalized so that $|E(t)|^2$ is an adimensional quantity indicating the number of photons in the internal cavity of the diode laser. The optical gain per time unit is given by $\Gamma G_N(N - N_{\mathrm{th}})$, where Γ is the optical confinement factor and $G_N(N - N_{\mathrm{th}})$ is the linearized gain of the carrier number, with G_N the differential gain and N_{th} the threshold carrier number of the solitary laser. The feedback is accounted for through the external-cavity round-trip time τ and the feedback parameter κ, defined as the square root of the power reflectivity of the external cavity, including the reflection at the output facet of the diode laser, relative to the reflectivity of such a facet. The other parameters in equations (8) have their usual meaning: α is the linewidth enhancement factor, τ_{in} is the internal-cavity round-trip time, Γ_0 represents the optical losses per time unit in the internal cavity, τ_{e} is the carrier lifetime and J is the carrier bias rate. The Lang–Kobayashi equations allow for only one external round trip, which is a good approximation in the case of weak to moderate feedback, as well as for arbitrary feedback levels with antireflection-coated lasers. We account for the absorptive and dispersive properties of the atomic vapour in the external cavity by including a frequency dependence in the definitions of the feedback parameters.

Equation (8*a*) describes the electric field within the internal cavity of the diode laser, at a reference plane placed just at the output facet, taken as the origin for the longitudinal spatial coordinate. Let us assume that a stationary field $\mathcal{E}_i = E_i\exp(-\mathrm{i}\omega t)$ is incoming to the output facet from inside the diode cavity. If only one external-cavity round trip is

considered, the total reflected field $\mathcal{E}_r = E_r \exp(-\mathrm{i}\omega t)$ at this facet is

$$\mathcal{E}_r = \left\{ r + \left(1 - r^2\right) r_{\mathrm{ext}} \mathrm{e}^{-(\alpha^+(\omega)+\alpha^-(\omega))L_{\mathrm{abs}}} \mathrm{e}^{-\mathrm{i}[(\beta^+(\omega)+\beta^-(\omega))L_{\mathrm{abs}} - 2\omega L_{\mathrm{cav}}/c]} \right\} \mathcal{E}_i \tag{9}$$

where r and r_{ext} are the amplitude reflectivities of the output facet of the diode laser and the external reflector, respectively, L_{abs} is the length of the cell containing the vapour, and L_{cav} is the length of the external cavity. As introduced in the preceding section, $\alpha^{\pm}$ and $\beta^{\pm}$ are the absorption and dispersion coefficients for the laser beams propagating forward and backward through the atomic sample. In equation (9), we have assumed that the amplitude of the field propagating in the positive direction, which acts as a saturating pump field, and the amplitude of the retroreflected field, acting as a probe, change linearly with the penetration depth within the atomic vapour. This assumption is well justified for the probe field, the intensity of which is much smaller than the saturation intensities of the atomic transitions, while it holds only approximately for the saturating field. We notice that, however, as the atomic lines are Doppler broadened, saturation effects are weakened due to the fact that contributions from detuned atoms are included in the average interaction [18].

The effective amplitude reflectivity of the external cavity [9] is defined as the ratio $r_{\mathrm{eff}} = \mathcal{E}_r / \mathcal{E}_i$ and is related to the feedback parameters κ and τ as

$$r_{\mathrm{eff}} = r\left(1 + \kappa \mathrm{e}^{\mathrm{i}\omega\tau}\right). \tag{10}$$

From the comparison between equations (9) and (10), we obtain the following definitions:

$$\kappa(\omega) = \frac{\left(1 - r^2\right) r_{\mathrm{ext}}}{r} \mathrm{e}^{-(\alpha^+(\omega)+\alpha^-(\omega))L_{\mathrm{abs}}} \tag{11a}$$

$$\tau(\omega) = \frac{1}{c}\left\{ (n^+(\omega) + n^-(\omega))L_{\mathrm{abs}} + 2(L_{\mathrm{cav}} - L_{\mathrm{abs}}) \right\} \tag{11b}$$

where the refractive indices relative to the pump and probe fields are introduced, as

$$n^{\pm}(\omega) = 1 - \frac{c}{\omega}\beta^{\pm}(\omega). \tag{12}$$

With the use of the feedback parameters expressed by equations (11), the Lang–Kobayashi equations, in (8), contain an explicit dependence on the laser frequency ω, so that they hold only for monochromatic laser fields. Therefore, they can be used to find the stationary laser modes, even if they are no longer valid for the description of the global laser dynamics.

3.3. Laser modes in the presence of an intracavity atomic absorber

The steady-state solutions of equations (8) are of the form $E(t) = E_{\mathrm{s}} \exp[-\mathrm{i}(\omega_{\mathrm{s}} - \omega_0)t]$ and $N(t) = N_{\mathrm{s}}$. By substitution, we obtain the following conditions:

$$f(\omega_{\mathrm{s}}) = 0 \tag{13}$$

with

$$f(\omega) = \omega - \omega_0 + \frac{\kappa(\omega)}{\tau_{\mathrm{in}}} \sqrt{1 + \alpha^2} \sin[\omega\tau(\omega) - \arctan\alpha] \tag{14}$$

and

$$N_{\mathrm{s}} - N_{\mathrm{th}} = -\frac{2}{\Gamma G_N} \frac{\kappa(\omega_{\mathrm{s}})}{\tau_{\mathrm{in}}} \cos[\omega_{\mathrm{s}}\tau(\omega_{\mathrm{s}})] \tag{15a}$$

$$E_{\mathrm{s}}^2 = \frac{J - N_{\mathrm{s}}/\tau_{\mathrm{e}}}{\Gamma_0/\Gamma + G_N(N_{\mathrm{s}} - N_{\mathrm{th}})}. \tag{15b}$$

Equation (13) represents the phase condition imposed by the external cavity containing the atomic absorber and its solutions define the set of possible laser frequencies, for given

feedback parameters. We consider the length of the external cavity, which modifies the round-trip time τ, and the oscillation frequency ω_0 of the solitary laser as externally controlled parameters. In fact, both parameters are accessible experimentally, by changing the longitudinal position of the external reflector through the piezoelectric transducer, and varying the bias current or case temperature of the diode laser, respectively. In equation (15*a*), N_s represents the threshold carrier number associated with the oscillation frequency ω_s. The difference $N_s - N_{th}$ is proportional to the threshold gain. From equation (15*b*), we see that the carrier bias rate J required to obtain a given laser power P_s is reduced, as N_s diminishes with respect to N_{th}.

A steady-state solution of the Lang–Kobayashi equations, satisfying the external-cavity phase condition, represents a laser mode only if it is locally stable under small phase changes [10]. By substituting, in equations (8), the electric field expressed as $E(t) = E_s \exp\{-i[(\omega_s - \omega_0)t + \phi(t)]\}$, where ω_s and E_s satisfy equations (13) and (15), and developing the equations to the first order in the phase perturbation ϕ and its time derivative $\dot{\phi}$, which represents the istantaneous frequency change, we obtain

$$\left.\frac{df(\omega)}{d\omega}\right|_{\omega_s} \dot{\phi}(t) = g(\omega_s)[\phi(t) - \phi(t - \tau(\omega_s))] \tag{16}$$

where the function $g(\omega)$ is introduced as

$$g(\omega) = -\frac{\kappa(\omega)\tau(\omega)}{\tau_{in}}\sqrt{1+\alpha^2}\cos[\omega\tau(\omega) - \arctan\alpha]. \tag{17}$$

Looking for solutions of the form $\phi(t) = \phi_0 \exp(st)$, equation (16) gives

$$\left.\frac{df(\omega)}{d\omega}\right|_{\omega_s} s\tau(\omega_s) = g(\omega_s)\left[1 - e^{-s\tau(\omega_s)}\right]. \tag{18}$$

This equation has a solution for s real and less than zero if either

$$\left.\frac{df(\omega)}{d\omega}\right|_{\omega_s} > g(\omega_s) > 0 \tag{19}$$

or

$$\left.\frac{df(\omega)}{d\omega}\right|_{\omega_s} < g(\omega_s) < 0. \tag{20}$$

Conditions (19) and (20) represent the requirements for a stationary solution of the Lang–Kobayashi equations to be a possible oscillating mode. In the limit of feedback parameters independent of ω, these requirements are reduced to the usual stability condition [8] for the empty-cavity modes. A complete linear stability analysis, involving variations of all laser variables, i.e. the amplitude and phase of the electric field, and carrier number, has to be performed in order to investigate the dynamic stability of each mode.

In figures 6(*a*) and 7(*a*), equation (13) is solved graphically for different values of the control parameters. Figures 6(*b*) and 7(*b*) show the corresponding threshold carrier number variation $N_s - N_{th}$, as a function of the frequency. On each curve, the points satisfying conditions (19) and (20) are marked. The figures correspond to different lengths of the external cavity, $\bar{L}_{cav} + \Delta L_{cav}$, with $\bar{L}_{cav} = 46$ cm and $\Delta L_{cav} = 0.1\lambda$ in figure 6 and $\Delta L_{cav} = 0.06\lambda$ in figure 7, with a laser wavelength of $\lambda = 2\pi c/\omega_0$. The function $f(\omega)$, along with the threshold carrier number, presents narrow structures, corresponding to the atomic Lamb dips or crossover resonances, superimposed on a slower frequency dependence, characterized by oscillations at a frequency given by the free spectral range of the external cavity modified by the dispersion of the atomic vapour. The frequency interval covered by

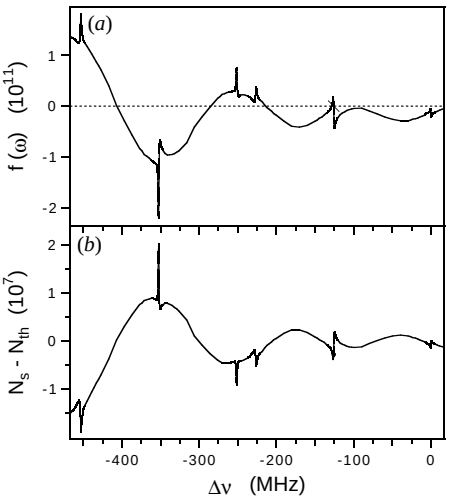

Figure 6. Graphic solution of equation (13), determining the steady-state oscillation frequencies, in (*a*), and stationary solution, as a function of the frequency, for the carrier number with respect to the solitary-laser threshold number (equation (15*a*)), in (*b*). The marker around -125 MHz indicates the steady-state solution which satisfies the stability conditions (19) and (20). For the parameters, the following values have been assumed: $G_N = 2.0 \times 10^4$ s^{-1}, $N_{\rm th} = 1.4 \times 10^8$, $\Gamma = 0.2$, $\alpha = 5.0$, $\tau_{\rm in} = 8.0 \times 10^{-12}$ s, $\Gamma_0 = 3.6 \times 10^{11}$ s^{-1}, $\tau_{\rm e} = 1.1 \times 10^{-9}$ s, $J = 1.2N_{\rm th}/\tau_{\rm e}$, $r = 0.56$, $r_{\rm ext} = 0.5$, $L_{\rm abs} = 4.0$ cm, $\omega_0 = 2.2 \times 10^{15}$ s^{-1} and $L_{\rm cav} = \bar{L}_{\rm cav} + \Delta L_{\rm cav}$, with $\bar{L}_{\rm cav} = 46$ cm and $\Delta L_{\rm cav} = 0.1\lambda$.

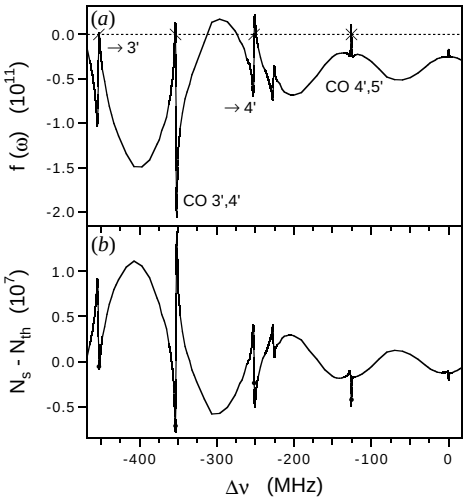

Figure 7. The same as in figure 6, except for the value of the control parameter $\Delta L_{\rm cav} = 0.06\lambda$. Several frequencies corresponding to different atomic resonances satisfy the phase condition (13) and the stability conditions (19) and (20). In (*a*), stable solutions located on points with positive (negative) slope, are marked by a slash / (backslash \). The cross $\times$ indicates a pair of closely spaced stable solutions, one on the rising side and the other on the descending side of the curve. Lamb dips and crossover resonances (CO) are labelled by the corresponding upper hyperfine states.

the horizontal axis is limited to a part of the Doppler-broadened spectrum, containing few Lamb dips or crossover resonances. Out of the atomic absorption spectrum, the feedback parameters are independent of the frequency, so that the stable solutions are those found for an empty external cavity, i.e. with a frequency separation equal to the cavity free spectral range. In figure 6, where the laser frequency is within the atomic absorption profile, one of the possible modes has its frequency clamped to the $4', 5'$ crossover resonance while other allowed modes lie outside the atomic spectrum. Figure 7 is obtained by changing, with respect to figure 6, the length of the external cavity by a fraction of the laser wavelength. In this figure, for fixed control parameters, several modes with oscillation frequencies locked to different atomic resonances are present simultaneously. From the left-hand side the laser modes correspond to the $4 \rightarrow 3'$ Lamb dip, the $3', 4'$ cross-over resonance, the $4 \rightarrow 4'$ Lamb dip and the $4', 5'$ cross-over resonance. By comparing figures 6(*a*) and 7(*a*) with the corresponding figures in (*b*), we can observe that the marked solutions which satisfy the stability conditions, are associated with a negative carrier number variation, i.e. a reduction of the lasing threshold and an increase of the optical gain with respect to the solitary laser. The situations illustrated in figures 6 and 7 are consistent with the observed optical spectra, shown in figures 3(*a*) and (*b*), respectively.

4. Summary and conclusions

The spectral behaviour of a diode laser subject to feedback from an external cavity containing a cell of Cs vapour in a saturation spectroscopy configuration was investigated experimentally and theoretically. We have focused our attention on the observed feature of multi-mode emission with oscillation frequencies clamped to different sub-Doppler atomic resonances within the D_2 line of the Cs absorber.

A rate equation model was developed, starting from the Lang–Kobayashi equations and including the effects of the absorptive and dispersive medium contained within the external cavity. The occurrence of multi-stability with frequency locking to different sub-Doppler atomic resonances, as observed experimentally, is accounted for by the model equations.

Despite the large amount of attention devoted to the issue of the absolute frequency stabilization of a diode laser through the inclusion of an atomic absorber within the feedback cavity, the question of the multi-mode emission induced by the absorber has never been addressed previously. The multi-stability discussed in this work suggests that the extended-cavity diode laser with an intracavity atomic absorber is also an interesting system from the point of view of the fundamental research on nonlinear dynamics and chaos. Recent achievements concerning the nonlinear behaviour of diode lasers with external feedback [12] point out that the simultaneous presence of several external-cavity modes gives rise to a peculiar chaotic regime. As the presence of the absorber substantially modifies the mode structure in the phase space of the extended-cavity laser system and also modifies the dynamic stability of the laser modes, novel features in the nonlinear dynamics involving the absorber-induced multi-mode operation should be expected.

Acknowledgments

The authors thank F Fuso for collaboration regarding the experimental configuration. This work was supported through a collaboration programme between the Centre National de la Recherche Scientifique (CNRS) of France and the Consiglio Nazionale delle Ricerche (CNR) of Italy. The Laboratoire de Spectroscopie Hertzienne is Unité de Recherche Associée au CNRS #249.

References

[1] Iannelli J, Shevy Y, Kitching J and Yariv A 1993 *IEEE J. Quantum Electron.* **QE-29** 1253 and references therein
[2] Cuneo C J, Maki J J and McIntyre D H 1994 *Appl. Phys. Lett.* **64** 2625
[3] Yariv A, Nabiev R and Vahala K 1990 *Opt. Lett.* **15** 1359
Shevy Y, Iannelli J, Kitching J and Yariv A 1992 *Opt. Lett.* **17** 661
Kitching J, Boyd R, Yariv A and Shevy Y 1994 *Opt. Lett.* **19** 1331
[4] Lee W D and Campbell J C 1991 *Appl. Phys. Lett.* **58** 995
Lee W D, Heuring J J, Campbell J C, Buell W F and Davis C L 1993 *Appl. Phys. Lett.* **63** 1026
[5] Cyr N, Breton M, Têtu M and Thériault S 1991 *Opt. Lett.* **16** 1298
[6] Kozuma M, Kourogi M, Ohtsu M and Hori H 1992 *Appl. Phys. Lett.* **61** 1895
[7] Liu Z D, Bloch D and Ducloy M 1994 *Appl. Phys. Lett.* **65** 274
[8] See, for instance, Tromborg B, Osmundsen J H and Olesen H 1984 *IEEE J. Quantum Electron.* **QE-20** 1023
Mørk J, Tromborg B and Mark J 1992 *IEEE J. Quantum Electron.* **QE-28** 93
Levine A M, van Tartwijk G H M, Lenstra D and Erneux T 1995 *Phys. Rev.* A **52** R3436
[9] Lang R and Kobayashi K 1980 *IEEE J. Quantum Electron.* **QE-16** 347
[10] Mørk J and Tromborg B 1990 *IEEE Photon. Technol. Lett.* **2** 21
Mørk J, Semkov M and Tromborg B 1990 *Electron. Lett.* **26** 609
Lenstra D 1991 *Opt. Commun.* **81** 209

[11] Masoller C 1994 *Phys. Rev.* A **50** 2569
[12] Sano T 1994 *Phys. Rev.* A **50** 2719
van Tartwijk G H M, Levine A M and Lenstra D 1995 *IEEE Sel. Top. Quantum Electron.* **1** 466
Fischer I, van Tartwijk G H M, Levine A M, Elsässer W, Göbel E and Lenstra D 1996 *Phys. Rev. Lett.* **76** 220
[13] Cerboneschi E, de Tomasi F and Arimondo E 1993 *Nonlinear Dynamics in Lasers and Optical Systems* (*SPIE* **2099**) p 183
de Tomasi F, Cerboneschi E and Arimondo E 1994 *IEEE J. Quantum Electron.* **QE-30** 2277
[14] Wieman C E and Hollberg L 1991 *Rev. Sci. Instrum.* **62** 1
[15] Zorabedian P 1994 *IEEE J. Quantum Electron.* **QE-30** 1542
[16] Schmidt O, Knaak K-M, Wynands R and Meschede D 1994 *Appl. Phys.* B **59** 167
[17] See, for instance, Hänsch T W, Shahin I S and Schawlow A L 1971 *Phys. Rev. Lett.* **27** 707
Svanberg S, Yan G-Y, Duffey T P and Schawlow A L 1986 *Opt. Lett.* **11** 138
[18] Meystre P and Sargent M III 1990 *Elements of Quantum Optics* (Berlin: Springer)